TD-DMRG coupled with n-mode representation potentials for the excited state radiationless decay rate: formalism and application to azulene

Jiajun Ren,[1] Yuanheng Wang,[1] Weitang Li,[1] Tong Jiang,[1] and Zhigang Shuai[1, a)]

MOE Key Laboratory of Organic OptoElectronics and Molecular Engineering,

Department of Chemistry, Tsinghua University, Beijing 100084,

People's Republic of China

(Dated: 15 August 2021)

We propose a method for calculating the nonradiative decay rates for polyatomic molecules including anharmonic effects of the potential energy surface (PES) in the Franck-Condon region. The method combines the n-mode representation method to construct the ab initio PES and the nearly exact time-dependent density matrix renormalization group method (TD-DMRG) to simulate quantum dynamics. In addition, in the framework of TD-DMRG, we further develop an algorithm to calculate the final-state-resolved rate coefficient which is very useful to analyze the contribution from each vibrational mode to the transition process. We use this method to study the internal conversion (IC) process of azulene after taking into account the anharmonicity of the ground state PES. The results show that even for this semi-rigid molecule the intramode anharmonicity enhances the IC rate significantly, and after considering the two-mode coupling effect, the rate increases even further. The reason is that the anharmonicity enables the C-H vibrations to receive electronic energy while C-H vibrations do not contribute on the harmonic PES as the Huang-Rhys factor is close to 0.

a)Electronic mail: zgshuai@tsinghua.edu.cn

I. INTRODUCTION

The photophysical properties of molecules have long been of research interest.[1] Especially in the last three decades, with the invent of organic light-emitting diode (OLED),[2] luminescent molecules have attracted continuous attention from academia and industry. One of the most influential factors on luminescent quantum efficiency is the intrinsic photophysical properties of the molecules. The famous Jablonski diagram gives the most basic physical picture of molecular photophysics. A molecule in the electronic excited state can emit photons radiatively back to the electronic ground state, or it can return to the ground state through an internal conversion (IC) process (transition within the same spin manifold) or an intersystem crossing (ISC) process (transition between different spin manifolds), in which the electronic energy is dissipated to vibrations in the form of heat. Both IC and ISC are nonradiative transition processes. The relative magnitude between the radiative transition rate k_r and the nonradiative transition rate k_nr ultimately determines the intrinsic quantum efficiency $\eta = k_\text{r}/(k_\text{r} + k_\text{nr})$ of the molecular material.[3] Therefore, it is crucial to develop theories and computational methods to predict the molecular nonradiative transition rates. In this work, we will focus on the rate theory of the IC process.
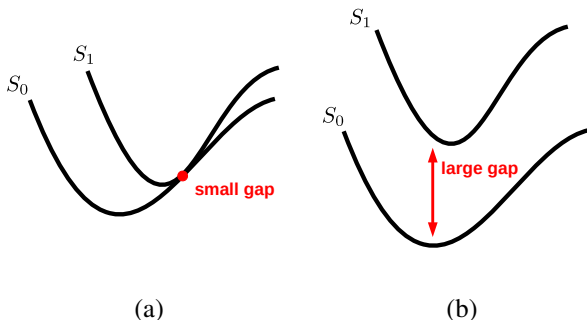

FIG. 1. Schematic diagram of two types of IC processes (a) The energy gap between the PESs is small, the NAC is large, and the IC process is ultrafast. (b) The energy gap between the PESs is large, the NAC is small, and the IC process is slow.

The molecular IC process is essentially a nonadiabatic process in which the Born-Oppenheimer (BO) approximation fails. The IC processes can be roughly classified into two types depending on the characteristics of the potential energy surface (PES) (Fig. 1). In type I, the nonadiabatic coupling (NAC) constant is very large and thus IC is an ultrafast process with time scales in the order of fs to ps.[4] This usually occurs when the energy gap between electronic states is relatively

2

small, such as the case of avoided crossing or conical intersection (CI) between PESs. IC between electronic excited states (generally having small energy gaps) are usually considered to belong to this type; photochemical reactions far from the Franck-Condon (FC) region (generally having a low energy CI between the S_1 and S_0 states) are also of this type. In type II, the coupling between electronic states is relatively small, and the time scale of the IC process is in the order of ns. It is usually considered that IC from S_1 state to S_0 state (having a relatively large energy gap) in the FC region, which is far from CI, belongs to this type. Theoretically, due to the large NAC between the electronic states in type I, BO fails completely and thus the simulation of real-time nonadiabatic dynamics becomes necessary, including the full-quantum multi-configuration time-dependent Hartree (MCTDH) method,[5] the time-dependent density matrix renormalization group (TD-DMRG) method,[6,7] the semiclassical methods,[8,9] and the hybrid quantum-classical methods.[10,11] For the latter two, direct dynamics on the ab initio PES can be done in combination with ab initio electronic structure packages.[12–14] However, these real-time nonadiabatic quantum dynamics approaches are not applicable to the IC process of type II, mainly because the transition time is too long to simulate quantum dynamically. The long-time propagation is not only computationally intensive but also has no guarantee of accuracy. For type II, because the NAC is small, the initial and final states before and after the transition can still be considered as a BO state. The transition between them is triggered by the NAC as a perturbation, the rate of which can be calculated by Fermi's golden rule (FGR). It is worth noting that since the radiative transition rates of organic fluorescent molecules are usually on the time scale of ns, if the nonradiative process of the molecule falls into type I, the molecule either does not emit light or emits light with very low efficiency. Molecules with a high quantum efficiency generally belong to type II. Therefore, the theory applicable to type II is more relevant for predicting fluorescent molecules with high quantum efficiency.

Qualitative and semi-quantitative theories applicable to type II of IC process were established in the 1960s.[15–17] Lin established the above-mentioned theoretical framework for calculating the IC rate based on BO states and NAC as a perturbation,[16] which is later combined with ab initio electronic structure calculation to predict the nonradiative transition rate of real molecules.[18–20] In this theoretical framework, the PES of the ground and excited states are approximated as a multidimensional harmonic (HA) potential, accompanied by displacement, frequency difference (distortion), and mode-mixing (Duschinsky rotation effect) between the PESs. The Duschinsky rotation effect, which scrambles the harmonic modes, was found to be important to the IC process.[19,21] How-

3

ever, in this computational method, the vibrational modes are artificially divided into accepting and promoting modes, and the displacement of the promoting mode is approximated as 0, called the promoting mode approximation. Later, Shuai *et al.* derived an analytical rate formula in the time domain beyond the promoting mode approximation, which allows a rigorous treatment of displacement, distortion, and rotation between the ground and excited state PESs.[22,23] Calculations of the nonradiative transition rate for a series of polyatomic molecules show that this method enables quantitative prediction of the quantum efficiency of OLED molecules.[24]

The above computational methods are based on the harmonic approximation of the PES with the anharmonicity completely ignored. In the radiative transition process, this approximation may be valid, because most of the electronic energy is emitted through the form of light. Thus, the final vibrational state is of low energy and can only explore the low energy part of the PES, where the anharmonicity is believed to be negligible. On the contrary, in the IC process, since all the electronic excited energy needs to be received by the vibrations, they will be excited to high energy levels. Because the anharmonicity is very pronounced in the high energy part of the PES far from the equilibrium position, the anharmonic effect is very important for the IC process (see schematic diagram Fig. 2). Lin's original work in 1966[16] has already pointed out the qualitative role of anharmonicity: it scrambles the harmonic mode (similar to the Duschinsky rotation effect) and thus is very important for vibrational relaxation; in addition, anharmonicity changes the vibrational wavefunction of the final states, which in turn changes the FC factor. In fact, these two factors are closely related.
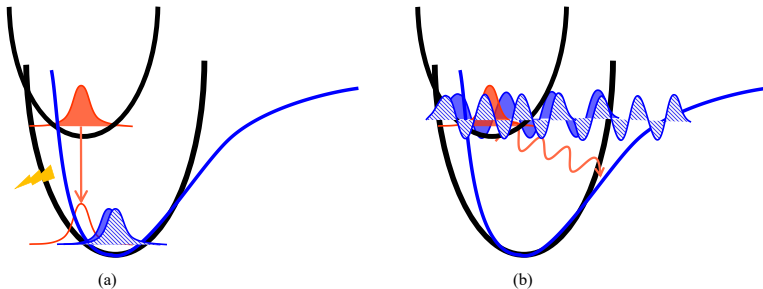

(a)   (b)

FIG. 2. Schematic diagram of the PESs and the wavefunctions of the initial and final vibrational states during the (a) radiative transition process (b) internal conversion process. The initial state is in orange, and the final state is in blue (filled ones are on the harmonic potential, and dashed ones are on the Morse potential).

In the framework of the FGR rate theory, the quantitative theoretical study of the anharmonic effect on the molecular IC process has only started in the last decade.[25–30] Humeniuk *et al.* used a time-independent (TI) approach under the Morse potential model to obtain the anharmonic vibrational wavefunction by exact diagonalization and then calculated the IC rate of coumarin molecules by means of the sum-of-states (SOS) method.[28] They found that, compared with HA PES, the Morse PES significantly increases the IC rate when the electronic excitation energy is large. However, for real molecules, the computational cost for SOS calculations increases exponentially with the number of atoms and thus the method is not scalable. A more promising approach is to use time-dependent (TD) methods. Zhu *et al.* used the second-order cumulant expansion method to consider the anharmonicity effect (introduced through the high-order force constants at the equilibrium position) on the vibrationally resolved electronic spectra and the rate of charge transfer.[25] This method can be directly extended to the calculation of IC rate. Pollak *et al.* proposed a semiclassical approach to calculate the IC rate on the anharmonic PES, and they calculated the IC rate for the Morse potential model[26] and formaldehyde.[27] The biggest advantage of this approach is that it is able to do on-the-fly calculations. Recently, we proposed to simulate the dynamics on the anharmonic PES by the full-quantum TD-DMRG method, the effectiveness of which has been proved on the Morse PES as well as the uncoupled single-mode anharmonic PES of real molecules.[30]

In addition to the accurate quantum dynamics method, another difficulty in the calculation of the nonradiative transition rate on the anharmonic PES for a real polyatomic molecule lies in how to construct the PES. One approach is to make a high-order Taylor expansion of the PES at the equilibrium position by calculating the high-order force constants. This approach is relatively cheap and is used more often in calculating the anharmonic vibrational frequencies of semi-rigid polyatomic molecules of medium to large sizes, especially in combination with the vibrational second-order perturbation theory and quasi fourth-order force constant.[31,32] However, the problem with the Taylor expansion form of PES is that it has a large error away from the reference point, and more seriously, it often introduces an artificial "potential hole". If the potential barrier between the reference point and artificial hole is not high enough, the wavepacket may collapse into this artificial hole, which is disastrous for the dynamics. Another approach is the multi-mode expansion, which is called *n*-mode representation (*n*-MR) by expanding the PES into a sum of one-mode potentials, two-mode potentials, three-mode potentials, etc.[33,34] The advantage of this approach is that the real PES can be approximated by a low-level expansion, making the number

5

of coupled modes in the approximated PES smaller. However, this approach requires a scan of the PES when obtaining each term, and thus is more computationally intensive for large systems with a high expansion order. The most accurate method is to fit the global PES directly. Previously, this method was only applicable to molecules with a few atoms, but with the development of deep machine learning over the years, the global PES can be obtained for medium-sized systems.[35,36] However, the obtained PES is generally not of a sum-of-products (SOP) form and thus cannot be directly used in the high-dimensional dynamics methods like multilayer MCTDH,[37] TD-DMRG, etc. Comparing the advantages and disadvantages of these PES construction methods, we propose to combine n-MR method and TD-DMRG method to calculate the nonradiative transition rate of real polyatomic molecules at the ab initio level.

The remaining sections of this paper are arranged as follows: in section II, the framework of rate theory, the methods of PES construction, TD-DMRG dynamics simulation, and the computation of final-state-resolved (FSR) transition rates will be presented in detail. In section III, the anharmonic effect on the IC rate from S_1 to S_0 of the azulene molecule in the FC region will be investigated and discussed as an example. Finally, conclusions and outlooks will be given.

II. THEORY AND METHODOLOGY

A. Two-state molecular Hamiltonian and rate theory under perturbation approximation

When NAC is relatively small, the initial and final states can be approximated by BO states, respectively. In addition, the contribution of the molecular vibrational motion to the electronic transition is dominant during IC, while the effect of molecular rotation can usually be ignored. By introducing the Eckart condition,[38] the coupling between vibration and rotation can be minimized, and thus only the vibrations need to be considered. Combining these two points, the initial and final states (i for the initial state and f for the final state) can be represented as

$$\Psi_{i/f}(\boldsymbol{r}, \boldsymbol{q}) = \phi_{i/f}(\boldsymbol{r}; \boldsymbol{q}) X_{i/f}(\boldsymbol{q}) \tag{1}$$

$\phi_{i/f}(\boldsymbol{r}; \boldsymbol{q})$ is the eigenstate of the electronic Hamiltonian under the nuclear configuration $\boldsymbol{q}$. $\boldsymbol{r}$ is the coordinates of electrons. $\boldsymbol{q} = q_1, q_2, \cdots, q_N$ are the vibrational coordinates of the system. The vibrational Hamiltonian is

$$\hat{H}_{i/f} = \hat{T} + V_{i/f}(\boldsymbol{q}) \tag{2}$$

$\hat{T}$ is the kinetic energy operator of the vibrational motions. $X_{i/f}(\boldsymbol{q})$ is the vibrational eigenstate on the adiabatic PES $V_{i/f}(\boldsymbol{q})$ (the energy reference is the minimum of each PES). The use of normal coordinates at the equilibrium structure is very suitable for semi-rigid systems. The first advantage is that the kinetic energy operator is very simple, $\hat{T} = \sum_{l=1}^{N} -\frac{1}{2} \frac{\partial^2}{\partial q_l^2}$ (in the following expressions, we use atomic units). In addition, the coupling between modes is small, which will be beneficial for constructing PES and simulating dynamics later. Due to the possible displacements, torsions and rotations between the initial PES and final PES, the two sets of normal coordinates are not the same and the relation between them is

$$q_{i,m} = \sum_l J_{ml} q_{f,l} + \Delta q_{i,m} \tag{3}$$

where $\boldsymbol{J}$ is called the Duschinsky rotation matrix and $\Delta \boldsymbol{q}$ is the projection of the displacement between the initial and final state equilibrium structures in the direction of the normal mode. The Huang-Rhys (HR) factor is defined as $S_{i/f,m} = \frac{1}{2} \omega_{i/f,m} \Delta q_{i/f,m}^2$, characterizing the strength of the electron-vibrational coupling. At the ab initio level, the methods to obtain $\boldsymbol{J}$ and $\Delta \boldsymbol{q}$ for polyatomic molecules are well-established [39,40]. In the following, $\boldsymbol{q}_{i/f}$ is assumed to be the normal coordinates. After considering NAC between the two electronic states as $\hat{H}_1$, $\Psi_{i/f}$ is no longer stationary. Commonly, only the first-order derivative term of NAC is considered, and the second-order derivative is neglected. The NAC between two BO PESs is

$$\hat{H}_1 = -\sum_l F_{fi}^l(\boldsymbol{q}) |\phi_f\rangle \langle \phi_i| \frac{\partial}{\partial q_l} + \text{h.c.} \tag{4}$$

$$F_{fi}^l(\boldsymbol{q}) = \langle \phi_f| \frac{\partial}{\partial q_l} |\phi_i\rangle_r \tag{5}$$

In the FC region far from CI, the NAC matrix element $F_{fi}^l(\boldsymbol{q})$ is small and also varies very smoothly. It is often to adopt the Condon approximation at the reference position to approximate $F_{fi}^l(\boldsymbol{q})$ as a constant independent of the nuclear configuration, i.e. $F_{fi}^l(\boldsymbol{q}) = F_{fi}^l(\boldsymbol{q}^{\text{ref}})$.

In addition to the approximation that the initial and final states can be represented by BO states, another assumption is that the rate of vibrational relaxation on the initial PES is much faster than the electronic transition, so that the initial state is in a thermal equilibrium distribution. This assumption is generally valid for fluorescent molecules because the vibrational relaxation time is roughly in the order of ps, while the excited state lifetime is roughly in the order of ns. Under the condition that both approximations hold, the IC rate can be calculated by FGR rate theory, which

is

$$k_{ic} = 2\pi \sum_{uv} P_u |H_{1,fv,iu}|^2 \delta(E_{iu} + \Delta E_{ad} - E_{fv}) \tag{6}$$

$$= 2\pi \sum_{uv} P_u |\sum_l F_{fi}^l \langle X_{fv}(\boldsymbol{q})| \frac{\partial}{\partial q_l} |X_{iu}(\boldsymbol{q})\rangle|^2 \delta(E_{iu} + \Delta E_{ad} - E_{fv}) \tag{7}$$

iu denotes the uth vibrational eigenstate of the initial PES and fv denotes the vth vibrational eigenstate of the final PES, whose eigenenergies are E_{iu} and E_{fv}, respectively. $P_u = \frac{e^{-\beta E_{iu}}}{Z}$ is the Boltzmann distribution of the initial state at the temperature of $\beta = 1/k_B T$. ΔE_{ad} is the adiabatic excitation energy between the PESs. For a general PES, the vibrational eigenfunction $X(\boldsymbol{q})$ is a high-dimensional wavefunction and it is very difficult, if not impossible, to compute each of them. If there is no coupling between the modes ($V(\boldsymbol{q}) = \sum_l V(q_l)$), the vibrational eigenstate can be written in the form of a Hartree product of the single-mode eigenstates, and the energy is also a summation of the individual mode eigenenergies

$$X_{iu}(\boldsymbol{q}_i) = \prod_l \chi_{iu_l}(q_{i,l}), \ E_{iu} = \sum_l \varepsilon_{iu_l} \tag{8}$$

$$X_{fv}(\boldsymbol{q}_f) = \prod_l \chi_{fv_l}(q_{f,l}), \ E_{fv} = \sum_l \varepsilon_{fv_l} \tag{9}$$

Additionally, if there is no mode-mixing ($\mathbf{J} = \mathbf{I}$, $\boldsymbol{q}_i = \boldsymbol{q}_f + \Delta\boldsymbol{q}$), the above equation can be further simplified as

$$k_{ic} = 2\pi \sum_{\substack{u_1,u_2,\cdots,u_N, \\ v_1,v_2,\cdots,v_N}} P_{u_1 u_2 \cdots u_N} \left| \sum_l F_{fi}^l \langle \chi_{fv_l}(q_l)| \frac{\partial}{\partial q_l} |\chi_{iu_l}(q_l + \Delta q_l)\rangle \prod_{k \neq l} \langle \chi_{fv_k}|\chi_{iu_k}\rangle \right|^2 \delta(E_{iu} + \Delta E_{ad} - E_{fv}) \tag{10}$$

q_l is called the promoting mode, contributing to the transition of the electronic state. Only those modes with nonzero NAC constant can behave as the promoting mode. The other modes are called the accepting modes. As the name implies, for multi-mode molecules, the electronic energy mainly dumps into the accepting modes. In addition, the magnitude of the FC factor between the final and initial states of the accepting modes satisfying the energy conservation condition mainly determines the IC rate. However, even though the modes are uncoupled, the calculation of the above equation using the SOS approach has exponential complexity. Hence, it is preferred to use the TD approach, in which the δ function is expressed as

$$\delta(E_{iu} + \Delta E_{ad} - E_{fv}) = \frac{1}{2\pi} \int_{-\infty}^{\infty} e^{i(E_{iu} + \Delta E_{ad} - E_{fv})t} \, dt \tag{11}$$

8

The rate can be written as the integral of the autocorrelation function of $\hat{H}_1$ in the time domain

$$k_{\text{ic}} = \int_{-\infty}^{\infty} e^{i\Delta E_{\text{ad}}t} C(t)\, dt \tag{12}$$

$$C(t) = \langle \hat{H}_1(t)\hat{H}_1 \rangle_T = \text{Tr}\left(\frac{e^{-\beta \hat{H}_i}}{Z(\beta)} e^{i\hat{H}_i t} \hat{H}_1 e^{-i\hat{H}_f t} \hat{H}_1\right) \tag{13}$$

where $Z(\beta) = \text{Tr}(e^{-\beta \hat{H}_i})$. For the case in which both PESs are harmonic, the time correlation function (TCF) $C(t)$ in Eq. (13) has an analytical formula.[22] For general PESs, $C(t)$ needs to be computed numerically by dynamics methods. The challenges for the calculation of the IC rate at ab initio level of real molecules are the construction of PES in Eq. (2) and the simulation of the dynamics in Eq. (13).

Finally, it is worth noting that for very flexible molecules, such as molecules whose PESs have many local minima (multiple conformations) with close energy, or molecules whose vibrations have a large amplitude of motion, using normal coordinates to construct PES and to do dynamics is no longer efficient, because the coupling between normal modes will be very large. In these cases, it is better to use curvilinear internal coordinates related to the molecular structure, but the kinetic energy operator in curvilinear coordinates is generally very complicated. The method to calculate the nonradiative transition rate using curvilinear coordinates is still under development and deserves further study.

B. Construction of molecular potential energy surface

The n-MR PES has expression

$$V(q_1, q_2, \cdots, q_N) = V^{(0)}(\boldsymbol{q}^{\text{ref}}) + \sum_i V^{(1)}(q_i; q_{l\neq i}^{\text{ref}})$$

$$+ \sum_{i<j} V^{(2)}(q_i, q_j; q_{l\neq ij}^{\text{ref}}) + \cdots \tag{14}$$

$$V^{(1)}(q_i; q_{l\neq i}^{\text{ref}}) = V(q_i; q_{l\neq i}^{\text{ref}}) - V^{(0)}(\boldsymbol{q}^{\text{ref}}) \tag{15}$$

$$V^{(2)}(q_i, q_j; q_{l\neq ij}^{\text{ref}}) = V(q_i, q_j; q_{l\neq ij}^{\text{ref}}) - V^{(1)}(q_i; q_{l\neq i}^{\text{ref}})$$

$$- V^{(1)}(q_j; q_{l\neq j}^{\text{ref}}) - V^{(0)}(\boldsymbol{q}^{\text{ref}}) \tag{16}$$

$$\cdots$$

Eq. (14) is an incremental expression, in which $V^{(0)}$ is the energy of the reference point. The second terms $V^{(1)}$ and third terms $V^{(2)}$ are the incremental one-mode and two-mode potentials.

$(q_i; \boldsymbol{q}^{\mathrm{ref}}_{l \neq i})$ indicates that only q_i can be different from the reference point. Hence, $V(q_i; \boldsymbol{q}^{\mathrm{ref}}_{l \neq i})$ in Eq. (15) corresponds to a one-dimensional (1D) curve of PES across the reference point along q_i. Similarly, $V(q_i, q_j; \boldsymbol{q}^{\mathrm{ref}}_{l \neq ij})$ in Eq. (16) represents the two-dimensional (2D) surface of PES across the reference point along q_i, q_j. However, the higher-order terms contain contributions from lower-order terms, for example, the 2D surface $V(q_i, q_j; \boldsymbol{q}^{\mathrm{ref}}_{l \neq ij})$ already contains two 1D curves $V(q_i; \boldsymbol{q}^{\mathrm{ref}}_{l \neq i})$, $V(q_j; \boldsymbol{q}^{\mathrm{ref}}_{l \neq j})$ and the energy of the reference point. Therefore, in the incremental expression Eq. (14), the contribution of the lower-order terms needs to be deducted from each $V^{(n)}$ to avoid double-counting. Obviously when any of the variable coordinates in $V^{(n)}$ is in the reference point, $V^{(n)}(q_i, q_j = q^{\mathrm{ref}}_j, q_k \cdots; \boldsymbol{q}^{\mathrm{ref}}_{l \neq ijk\ldots}) = 0$. As the expansion order n increases, the approximate PES gradually approaches the exact one. This multi-mode expansion is exact when expanding to N-mode potential $V^{(N)}$. In practice, only $n < N$ order is usually enough to converge. Assuming that 10 points are scanned in each coordinate, the number of single points needed to compute an n-mode PES of a system having N modes is about $C^n_N 10^n$. One advantage of n-MR is that, since it is a semi-global PES, there is no artificial hole. Another advantage is that since there are only at most n-mode coupled terms, it is relatively easy to fit them into a dynamics-friendly SOP form after some post-processing, such as potfit[41] and function fitting. In the function fitting method, a set of functions for each mode is first defined $\{f^k(x)\}$ (k is the label for different functions), which can be the same or different for each mode. For simplicity, we use the same monomial for each mode as the fitting function, then k represents the power of the monomial, $k = 0, 1, 2, \cdots$.

$$f^k(x) = x^k \tag{17}$$

For each term $V^{(n)}$ in Eq. (14), it can be fitted to a polynomial of the form

$$\tilde{V}^{(n)}(q_{i_1}, \cdots, q_{i_n}) = \sum_{k_1, \cdots, k_n} C_{k_1, \cdots, k_n} f^{k_1}(q_{i_1}) \cdots f^{k_n}(q_{i_n}) \tag{18}$$

It is clear that $\tilde{V}^{(n)}$ has an analytical SOP form.

With n-MR method, two independent PESs $V_{\mathrm{i}}(\boldsymbol{q}_{\mathrm{i}})$ and $V_{\mathrm{f}}(\boldsymbol{q}_{\mathrm{f}})$ in Eq. (2) can be constructed in the normal coordinates of each state. However, it is necessary to work in a single coordinate system in the dynamics. Hence, the PESs should be further transformed into one set of normal coordinates according to the relation Eq. (3). For example, in the following we will work in the normal coordinates of the final state and the initial PES is reexpressed as

$$V_{\mathrm{i}}(\boldsymbol{q}_{\mathrm{i}}) = V_{\mathrm{i}}(\mathbf{J}\boldsymbol{q}_{\mathrm{f}} + \Delta \boldsymbol{q}_{\mathrm{i}}) = V'_{\mathrm{i}}(\boldsymbol{q}_{\mathrm{f}}) \tag{19}$$

In principle, instead of using Eq. (3) to rewrite $V_i(q_i)$ in q_f to obtain $V'_i(q_f)$, it is also possible to scan V_i directly along q_f. But in doing so, V_i may require a higher order n-MR to achieve satisfactory accuracy. For example, the potential energy term λq_{i1}^2 in 1-MR PES with initial state normal coordinates becomes $\lambda \sum_{lm}(S_{l1}q_{fl} + \Delta q_{i1})(S_{m1}q_{fm} + \Delta q_{i1})$ with final state normal coordinates, which includes two-mode potential energy terms appearing in 2-MR PES.

C. TD-DMRG quantum dynamics method

The wavefunction ansatz in TD-DMRG is

$$|\Psi\rangle = \sum_{\sigma} C_{\sigma_1 \sigma_2 \ldots \sigma_N} |\sigma_1 \sigma_2 \ldots \sigma_N\rangle \tag{20}$$

$$= \sum_{a\sigma} A_{a_1}^{\sigma_1} A_{a_1,a_2}^{\sigma_2} \ldots A_{a_{N-1}}^{\sigma_N} |\sigma_1 \sigma_2 \ldots \sigma_N\rangle \tag{21}$$

$|\sigma_i\rangle$ is the orthonormal primitive basis for each vibrational mode q_i, which is called the physical bond with dimension d. In this work, we use simple harmonic oscillator eigenfunctions (SHO) as the primitive basis functions. Since the full rank coefficients $C_{\sigma_1 \sigma_2 \ldots \sigma_N}$ are approximated as the product of a chain of rank-3 matrices (tensors) $A_{a_{i-1},a_i}^{\sigma_i}$, this ansatz is called matrix product state (MPS).[42] The size of a_i connecting adjacent tensors is called the (virtual) bond dimension, denoted as M_S. The accuracy of an MPS approximating the exact wavefunction can be systematically improved by increasing M_S. Akin to MPS, a common operator $\hat{O}$ can be exactly decomposed into a matrix product form with virtual bond dimension M_O, called matrix product operator (MPO).

$$\hat{O} = \sum_{w,\sigma,\sigma'} W_{w_1}^{\sigma'_1 \sigma_1} W_{w_1,w_2}^{\sigma'_2 \sigma_2} \ldots W_{w_{N-1}}^{\sigma'_N \sigma_N} |\sigma'_1 \sigma'_2 \ldots \sigma'_N\rangle \langle \sigma_N \sigma_{N-1} \ldots \sigma_1| \tag{22}$$

The potential energy term (Eq. (18)) and the other operators (Eq. (2) (4)) in the previous section can be constructed into MPOs using the automatic construction algorithm proposed in our former work.[43] Within the MPS/MPO framework, it is straightforward to represent $\hat{O}|\Psi\rangle$ as another enlarged MPS with bond dimension $M_O M_S$.

$$\hat{O}|\Psi\rangle = \sum_{w,a,\sigma'} A'^{\sigma'_1}_{\{w,a\}_1} A'^{\sigma'_2}_{\{w,a\}_1,\{w,a\}_2} \ldots A'^{\sigma'_N}_{\{w,a\}_{N-1}} |\sigma'_1 \sigma'_2 \ldots \sigma'_N\rangle \tag{23}$$

$$A'^{\sigma'_i}_{\{w,a\}_{i-1},\{w,a\}_i} = \sum_{\sigma_i} W_{w_{i-1},w_i}^{\sigma'_i \sigma_i} A_{a_{i-1},a_i}^{\sigma_i} \tag{24}$$

A similar expression is available for operator multiplication. In TD-DMRG, there are many schemes that can evolve an MPS according to the time-dependent Schrödinger equation.[44] In this

work, we use the second-order projector splitting scheme (PS) based on the time-dependent variational principle. This scheme is more accurate and efficient than the others according to our former experience. The detailed algorithm can be found in the original PS work[45] or our previous work.[46]

At $T = 0$, the TCF $C(t)$ (Eq. (13)) can be further simplified as

$$C(t) = e^{iE_{i0}t} \langle X_{i0}|\hat{H}_1 e^{-i\hat{H}_f t}\hat{H}_1|X_{i0}\rangle = e^{iE_{i0}t} \langle X_f(t/2)^*|X_f(t/2)\rangle \tag{25}$$

$$|X_f(t/2)\rangle = e^{-i\hat{H}_f t/2}\hat{H}_1|X_{i0}\rangle \tag{26}$$

The asterisk represents complex conjugate. $|X_{i0}\rangle$ is the lowest vibrational eigenstate on the initial PES, which can be calculated by the standard DMRG ground state algorithm, i.e., iteratively optimizing each local matrix A^{σ_i} while keeping the others unchanged.[42,47] The initial state $\hat{H}_1|X_{i0}\rangle$ of the dynamics is calculated according to Eq. (23). At $T = 0$, it is possible to evolve only the dynamics for $t/2$ to obtain TCF at t thus reducing the computational cost.

At finite temperature, it is able to obtain the density matrix at thermal equilibrium $\rho_\beta = \frac{e^{-\beta \hat{H}_i}}{Z(\beta)}$ by evolving the imaginary-time Schrödinger equation from $\tau = 0$ to $\tau = \beta/2$.[48]

$$-\frac{\partial}{\partial \tau}\rho(\tau) = \hat{H}\rho(\tau) \tag{27}$$

At infinitely high temperature ($\beta = 0$), the initial state $\rho(0)$ is defined to be a locally maximal entangled state satisfying the normalization condition $\langle\langle \rho(\tau)|\rho(\tau)\rangle\rangle = \mathrm{Tr}(\rho(\tau)^\dagger \rho(\tau)) = 1$, which is conveniently represented as an MPO with $M_O = 1$. To distinguish it from the MPO of a physical operator, we call the matrix product form of the density matrix as matrix product density matrix (MPDM).

$$\rho(0) = \frac{e^{-0\hat{H}_i}}{\sqrt{Z(0)}} = \prod_i \sum_{\sigma_i} \frac{1}{\sqrt{d}}|\sigma_i\rangle\langle\sigma_i| \tag{28}$$

After each evolution step along the imaginary axis, $\rho(\tau)$ needs to be normalized. The imaginary-time evolution finally yields $\rho(\beta/2) = e^{-\beta \hat{H}_i/2}/\sqrt{Z(\beta)} = \rho_\beta^{1/2}$. Hence, TCF in Eq. (13) can be reformulated as

$$C(t) = \mathrm{Tr}\left(\rho_\beta^{1/2} e^{i\hat{H}_i t}\hat{H}_1 e^{-i\hat{H}_f t}\hat{H}_1 \rho_\beta^{1/2}\right) = \mathrm{Tr}(\rho_i(t)^\dagger \hat{H}_1 \rho_f(t)) \tag{29}$$

where $\rho_f(t) = e^{-i\hat{H}_f t}\hat{H}_1\rho_\beta^{1/2}$ and $\rho_i(t) = e^{-i\hat{H}_i t}\rho_\beta^{1/2}$ is the density matrix obtained by the real-time evolution. It should be noted that in some papers, the density matrix is purified to a wavefunction according to the thermo field dynamics approach by introducing an auxiliary space, thus obtaining wavefunction-based equations of imaginary-time and real-time dynamics.[42,49] These two formulations are essentially equivalent to each other.

12

The main advantages of using TD-DMRG to simulate dynamics are (i) TD-DMRG is fully quantum and the accuracy can be systematically improved to achieve numerically exact results. (ii) The computational complexity of TD-DMRG algorithm is polynomial, rather than exponential, with respect to the number of atoms in the system.

D. Final-state-resolved rate coefficient

Besides the total transition rate, in this subsection, we will give an algorithm to calculate the numerically exact FSR rate coefficient for uncoupled final PES, such as HA PES, 1-MR PES. To the best of our knowledge, the only way to obtain the FSR rates so far was by expensive SOS methods.

According to Eq. (6), (11) and (29), the FSR rate can be expressed in the time domain as

$$k_{\boldsymbol{v}} = k_{\text{ic}}(\text{i} \to \text{f}\boldsymbol{v}) = \int_{-\infty}^{\infty} e^{i\Delta E_{\text{ad}}t} \text{Tr}(\rho_{\beta}^{1/2} e^{i\hat{H}_{\text{i}}t} \hat{H}_1 |X_{\text{f}\boldsymbol{v}}\rangle\langle X_{\text{f}\boldsymbol{v}}| e^{-i\hat{H}_{\text{f}}t} \hat{H}_1 \rho_{\beta}^{1/2}) \, dt \tag{30}$$

$$= \int_{-\infty}^{\infty} e^{i\Delta E_{\text{ad}}t} \langle X_{\text{f}\boldsymbol{v}}|\Gamma(t)|X_{\text{f}\boldsymbol{v}}\rangle \, dt \tag{31}$$

$$\Gamma(t) = \rho_{\text{f}}(t)\rho_{\text{i}}(t)^{\dagger}\hat{H}_1 \tag{32}$$

At $T = 0$,

$$\Gamma(t) = e^{iE_{i0}t} |X_{\text{f}}(t/2)\rangle\langle X_{\text{f}}(t/2)^*| \tag{33}$$

$\Gamma(t)$ is in the form of an MPDM and $\text{Tr}(\Gamma(t)) = C(t)$. Since $\Gamma(t)$ is the product of two MPDMs (Eq. (32)) or two MPSs (Eq. (33)), its bond dimension is $M_{\Gamma} = M_{\rho_{\text{i}}} M_{\rho_{\text{f}}} M_{\hat{H}_1}$ or $M_{\Gamma} = M_{X_{\text{f}}}^2$, which is usually a very large value. Thus, $\Gamma(t)$ needs to be compressed to reduce the computational cost and memory. In the case of uncoupled final PES, Eq. (9) holds, and $\boldsymbol{v} = v_1 v_2 \cdots v_N$. For HA PES, the eigenstate of a single mode $\chi_{\text{f}v_l}$ has an analytical form; for 1-MR PES, $\chi_{\text{f}v_l}$, called modal, can be calculated numerically by vibrational self-consistent field (VSCF).[50] If $\chi_{\text{f}v_l}$ is chosen to be the primitive basis in TD-DMRG ($|\sigma\rangle \equiv |v\rangle$),

$$\Gamma_{\text{diag}}(t)|_{\boldsymbol{\sigma}=\boldsymbol{v}} = \langle \prod_l \chi_{\text{f}v_l} | \Gamma(t) | \prod_l \chi_{\text{f}v_l} \rangle \tag{34}$$

$$= \sum_{\boldsymbol{w}} W_{w_1}^{v_1 v_1} W_{w_1,w_2}^{v_2 v_2} \cdots W_{w_{N-1}}^{v_N v_N} \tag{35}$$

$$= \sum_{\boldsymbol{w}} \tilde{W}_{w_1}^{v_1} \tilde{W}_{w_1,w_2}^{v_2} \cdots \tilde{W}_{w_{N-1}}^{v_N} \tag{36}$$

13

$\Gamma_{\text{diag}}(t)$ is the diagonal element with the primitive basis $\chi_{\text{f}v_l}$, which can be expressed as an MPS with $\tilde{W}_{w_{l-1},w_l}^{v_l} = W_{w_{l-1},w_l}^{v_l v_l}$. As a result, Eq. (31) can be written as

$$k_{\boldsymbol{v}} = \int_{-\infty}^{\infty} e^{i\Delta E_{\text{ad}}t}\Gamma_{\text{diag}}(t)|_{\boldsymbol{\sigma}=\boldsymbol{v}}\,dt \tag{37}$$

$$= \left(\int_{-\infty}^{\infty} e^{i\Delta E_{\text{ad}}t}\Gamma_{\text{diag}}(t)\,dt\right)\bigg|_{\boldsymbol{\sigma}=\boldsymbol{v}} \tag{38}$$

The integration of $\Gamma_{\text{diag}}(t)$ can be done by the trapezoidal algorithm and by using the symmetry of TCF,

$$I_{\text{half}} = \sum_{j=0}^{\infty} \frac{\tau}{2}\left[e^{i\Delta E_{\text{ad}}j\tau}\Gamma_{\text{diag}}(j\tau) + e^{i\Delta E_{\text{ad}}(j+1)\tau}\Gamma_{\text{diag}}((j+1)\tau)\right] \tag{39}$$

$$k_{\boldsymbol{v}} = I|_{\boldsymbol{\sigma}=\boldsymbol{v}} = (I_{\text{half}} + I_{\text{half}}^*)|_{\boldsymbol{\sigma}=\boldsymbol{v}} \tag{40}$$

where τ is the time-step. When calculating I_{half}, MPS compression is carried out after adding two MPSs. The coefficient of each configuration $\boldsymbol{v}$ in I is the rate with that configuration as the final state. If $\Gamma(t)$ and I_{half} are not compressed, $\sum_{\boldsymbol{v}} I = k_{\text{ic}}$. However, all the coefficients are implicit in the form of the matrix product. Because the number of final states is exponentially increased with the number of modes, it is impossible to obtain all $I|_{\boldsymbol{\sigma}=\boldsymbol{v}}$ explicitly. In fact, if we only care about those final configurations that contribute the most to the total IC rate, a sampling approach can be used. Inspired by the sampling algorithm and genetic algorithm used in the ab initio quantum chemistry DMRG to reconstruct configuration interaction wavefunction,[51,52] we propose a similar sampling algorithm to obtain the dominant configurations of I. We first define the occurrence probability of different occupation numbers for each mode during the total transition.

$$p_{v_l} = \sum_{\text{all } v_k, k \neq l} \frac{k_{v_1 v_2, \cdots, v_l, \cdots v_N}}{k_{\text{ic}}}$$

$$= \sum_{\text{all } v_k, k \neq l} \frac{1}{k_{\text{ic}}} A^{v_1} A^{v_2} \cdots A^{v_l} \cdots A^{v_N} \tag{41}$$

Here, A^{v_i} are the local matrices of I. Note that $\sum_{v_l} p_{v_l} = 1$. According to this probability distribution, the whole sampling procedure is

1. calculate I and then calculate p_{v_l} according to Eq. (41).

2. generate a random configuration $\boldsymbol{v}$, calculate its rate coefficient $k_{\boldsymbol{v}}$ and keep it if it is greater than a preset threshold ξ.

14

3. generate an integer random number k between 1 to N, and then mutate v_k of the current $\boldsymbol{v}$ according to the distribution $p_{v_k}.v_k'$ can be determined by generating a random number between [0,1] and check which interval it falls into. Repeat this step if $v_k' = v_k$.

4. calculate the rate $k_{\boldsymbol{v}'}$ of this $\boldsymbol{v}'$ and keep it if $k_{\boldsymbol{v}'} > \xi$ and it has not been kept yet. The probability to accept this mutation is defined as $p(\boldsymbol{v} \to \boldsymbol{v}') = \min(1, \frac{k_{\boldsymbol{v}'}}{k_{\boldsymbol{v}}})$, and then generate a $[0,1]$ random number to decide whether to accept this mutation. If accepted, the new $\boldsymbol{v} = \boldsymbol{v}'$ and then go back to step 3. Sampling ends if either the total number of the kept configurations or the sum of rate coefficient of the kept configurations reaches the preset value.

Since it is an approximation to use one MPS for all FSR rates, it is not guaranteed that all FSR rates are positive in the actual calculation. Therefore, in the later calculations, we set the threshold ξ to 0. In addition, although this algorithm is rigorous only for uncoupled final PES, it is possible that the Hartree product of VSCF modals is still a good approximation to the exact final states when the mode coupling in n-MR ($n > 1$) PES is relatively small.

Finally, it is worth emphasizing that the methods we propose to deal with the anharmonic PES of real molecules is not only applicable to IC rates, but can also be used for the calculation of the emission spectra (and the corresponding radiative transition rates) as well as for the calculation of ISC rates.
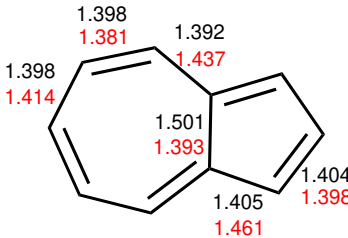
III. RESULTS AND DISCUSSIONS

FIG. 3. The chemical structure of azulene. The optimized C-C bond lengths of the S_0 state (black) and S_1 state (red) are also listed.

As a real example, we study the IC process of the azulene molecule from the S_1 state to the S_0 state. Azulene is the first experimentally discovered molecule with anti-Kasha rule luminescence,

which is from S_2 to S_0.[53,54] Its S_1 to S_0 IC rate is very fast, with experimental measurements of about 1-2 ps,[55,56] and thus the S_1 fluorescence quantum efficiency is very low. In our previous work, we found that azulene is a semi-rigid molecule, and even then there is a significant increase in the IC rate after considering the single-mode (intramode) anharmonicity compared to that on HA PES. In this work, the calculation is extended to the 2-MR PES to study the effect of mode coupling on the IC process.

The S_0 and S_1 structures of azulene are first optimized at (TD-)B3LYP/6-31G(d) level (all the following electronic structure calculations are done in Gaussian 16[57]). The total number of vibrational modes is 48. Although we do not add symmetry constraints, the optimized structure has C_{2v} symmetry. The S_0 and S_1 equilibrium structures are shown in Fig. 3. The adiabatic excitation energy is $16478.4\,\mathrm{cm}^{-1}$. The normal mode analysis at the S_0 and S_1 equilibrium structures is performed, and then the Duschinsky rotation matrix $\mathbf{J}$ and mode projection displacements Δq are calculated using the molecular material property prediction package (MOMAP).[58] Fig. 4a gives the HR factors along the normal modes of S_0 and S_1 states, respectively. For the S_0 state, the modes are numbered according to the vibrational frequencies, while the mode numbering for the S_1 state makes the Duschinsky rotation matrix as diagonalized as possible in accordance with the modes of the S_0 state. Fig. 4b shows the absolute values of the Duschinsky rotation matrix $\mathbf{J}$, and the red boxes highlight the mixing between modes with large HR factors. It can be seen that the mixing of modes 38 and 39 is very prominent. There are two main features of the azulene electron-vibrational coupling: first, the HR factors of all modes are less than 1, which can be classified into the weak coupling regime; second, the HR factors of high frequency C-H vibrations above $3000\,\mathrm{cm}^{-1}$ are small and negligible. The largest HR factor of the C-H vibrations is only 0.00126. In the displaced harmonic oscillator model, the mode with an HR factor of 0 (zero displacement) cannot be an accepting mode because $\langle \chi_{\mathrm{f}v} | \chi_{\mathrm{i}u} \rangle = \delta_{uv}$. Therefore, it can be expected that the ability of C-H vibrations to receive energy is weak on HA PES.[59] The C-H vibrations can only play the role of promoting mode triggering electronic transition. The projection of the NAC vector at the S_0 optimized structure onto the S_0 normal modes is shown in Fig. S1 (see Supporting Information). The NAC constant is larger in the C-C vibrational region and smaller in the C-H vibrational region. The Condon approximation is adopted to approximate NAC as a constant independent of the nuclear structure.

Since the thermal energy $k_{\mathrm{B}}T$ at room temperature is small relative to the vibrational frequency, the initial thermal equilibrium state is near the equilibrium position of the excited state PES, and
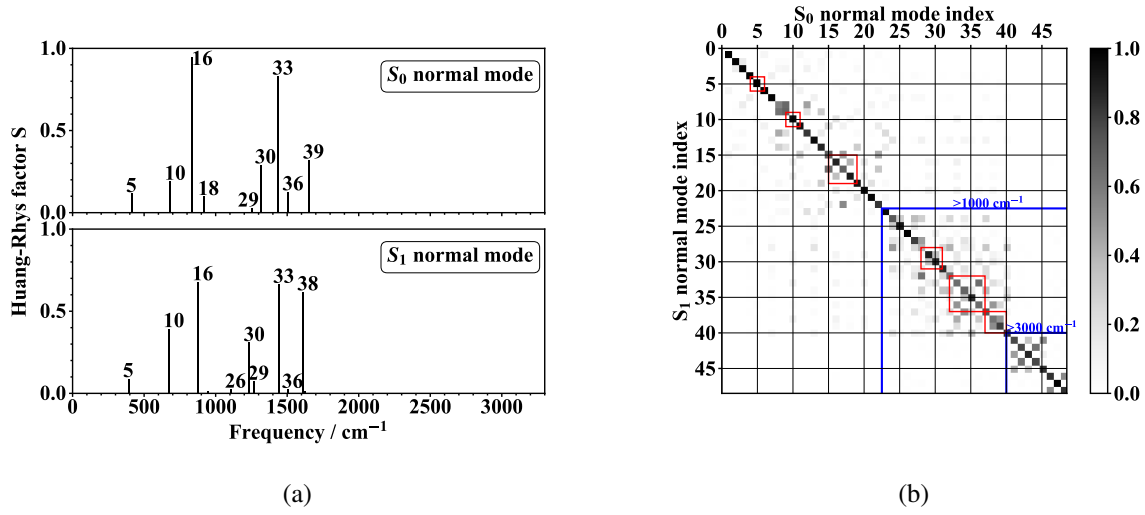
FIG. 4.   (a) The HR factors of S_0 normal modes (upper panel) and S_1 normal modes (lower panel). (b) The Duschinsky rotation matrix $|J_{ij}|$ between the S_0 and S_1 normal coordinates. The modes with large HR factors are highlighted by red boxes.

thus the anharmonic effect of the excited state PES is expected to be relatively small. On the contrary, according to the analysis above, the anharmonic effect of the ground state PES will be very significant. Therefore, we only consider the anharmonicity of the ground state PES, while the excited state is still approximated by HA PES. Along the normal modes of S_0 state, a 2-MR PES of the S_0 state is constructed using MidasCPP software[60] interfaced with Gaussian 16.[57] The single-point calculations are still performed at the B3LYP/6-31G(d) level. The adaptive density-guided approach (ADGA) is used to adaptively select the single points to be computed, which has the advantage of not requiring a predetermined range of each coordinate to be scanned.[61] The convergence of the PES obtained by ADGA is characterized by the lowest 7 modals for each mode computed by VSCF. More details of the ADGA method can be found in Ref. 61. The resulting n-MR PES is fitted with a polynomial up to 12th order, as in Eq. (18). For the 1-MR PES, a total of 665 single points are computed; for the 2-MR PES, a total of 201,825 single points are computed. The typical one-mode and two-mode cuts of the PES are shown in Fig. 5. To verify the accuracy of the n-MR PES, we compare the reorganization energy λ_{S_0} of the constructed S_0 PES. The reference energy is calculated by the so-called "four-point method". For λ_{S_0}, only two single-point calculations are required, $\lambda_{S_0} = E(S_0; S_1 \text{ opt geom}) - E(S_0; S_0 \text{ opt geom})$. Table I shows that the error of the PES decreases as the order of expansion increases.

We calculate the IC rates on the HA, 1-MR and 2-MR PESs using TD-DMRG. All calculations
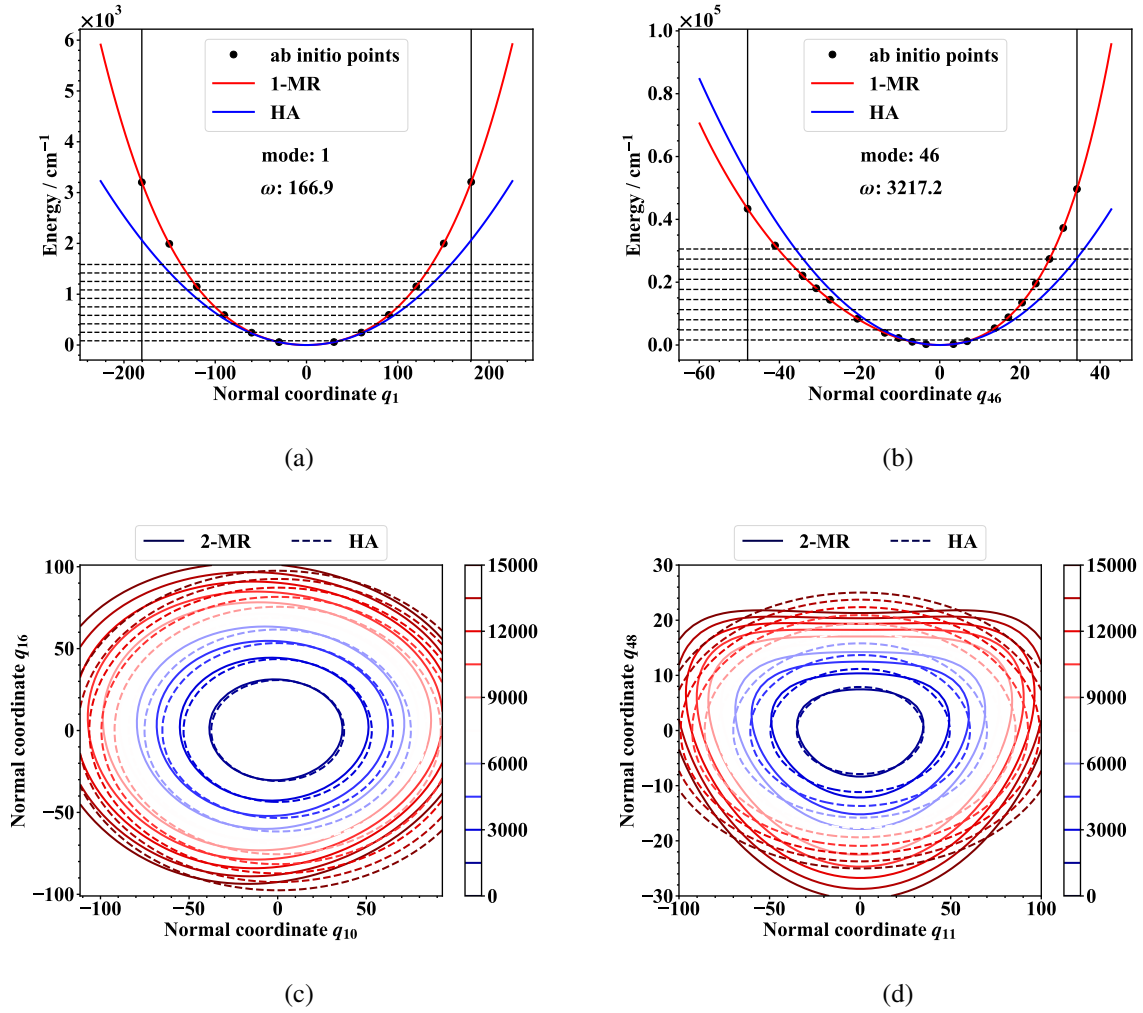
17

FIG. 5. (a)(b) The typical one-mode cuts of PES. The black circles are the ab initio points. The red line is the 1-MR energy curve fitting the ab initio points. The blue line is harmonic potential. The dashed horizon lines are the lowest 10 energy levels of the harmonic potential. (c)(d) The typical two-mode cuts of PES. The solid contour is the 2-MR surface and the dashed contour is the harmonic surface. The unit is cm^{-1}.

TABLE I. The reorganization energy calculated on different levels of S_0 PES. Units: cm^{-1}

	four-point method	HA	1-MR	2-MR
λ	3481.9	3399.2	3421.4	3495.7
error	-	-82.7	-60.5	13.8

18

are carried out with our in-house code Renormalizer.[62] The time-step is 0.25 fs, with a total evolution time of 425 fs. The primitive basis function for each mode is SHO basis up to 20 quanta ($d = 20$). Table II lists k_{ic} at 0K and 300K with different M_S. At 300K, the MPOs used for the TD-DMRG calculations with $M_S \geq 40$ are compressed to reduce the computational cost. The cutoff threshold used in singular value decomposition (SVD) is $\varepsilon = 10^{-6}$ after normalization of the singular values. With this cutoff, the error introduced through MPO compression is negligible. Since the thermal vibration correlation function (TVCF) method[24] (calculated using MOMAP package[58]) yields analytically exact solutions on HA PES, they are also listed for comparison. Because the directly calculated $C(t)$ does not dephase to 0 after finite time, it is multiplied by a broadening function $\tilde{C}(t) = C(t)g(t)$ in the time domain. The physical origin of this broadening function may be static disorder as well as dynamic disorder of the actual environment. Instead of a Lorentzian broadening function $g(t) = \exp(-\eta t)$ with $\eta = 100 \, \text{cm}^{-1}$ used in our former work, here a Gaussian broadening function $g(t) = \exp(-\eta^2 t^2/2)$ with $\eta = 100 \, \text{cm}^{-1}$ is adopted. The reason is that the Lorentzian broadening function has a very long tail in the frequency domain, decaying with $\frac{1}{\pi}\frac{\eta}{\Delta\omega^2+\eta^2}$ ($\Delta\omega$ is the detuning frequency). As a result, it will take into account many states that severely violate energy conservation but have large FC factors (Most are low energy states, which is evident in the FSR rate calculation). This behavior, although possible in the condensed phase, is clearly against the physical picture in the calculations of the single molecule model here. In comparison, the Gaussian broadening function decays exponentially in the frequency domain with $\frac{1}{\sqrt{2\pi}\eta}\exp(-\Delta\omega^2/2\eta^2)$, which can well satisfy the energy conservation. The choice of the broadening function and width have also been discussed in detail in Humeniuk's work.[28] For the same reason, they also found that the Gaussian broadening function has a small effect on the nonradiative transition rates, while the Lorentzian broadening has a large effect on it. Since the rate is related to the Gaussian broadening width, it is not feasible to directly compare the computational results with the experiments. Fortunately, it has little effect on the relative change of the rate due to anharmonicity, which is the main focus of this work. From the results in Table II, it shows that the TD-DMRG results converge very quickly with increasing M_S. For the mode-uncoupled HA PES and 1-MR PES, $M_S = 40$ is enough (if 1% error is required). For the coupled 2-MR PES, $M_S = 80$ will make the rate at 0 K converged, but is still not enough for the rate at 300 K. On HA PES, the numerical results of TD-DMRG can reproduce the analytically exact results of TVCF. The rate on 1-MR PES is about 200% of the rate on HA PES, indicating that the introduction of intramode anharmonicity will prominently accelerate the rate of IC. More significantly, the coupling between

19

modes has a greater effect on the IC rate: the rate on 2-MR PES is about 500% of the rate on HA PES. The physical picture of the quantitative results is that the mode coupling accelerates the vibrational relaxation and therefore the dephasing of the wavepackets on the excited and ground state PESs is much faster. To some extent, this mode coupling effect is similar to the Duschinsky rotation effect, both of which scramble the normal modes.

TABLE II. The internal conversion rate k_{ic} of azulene from S_1 to S_0 with harmonic PES, anharmonic 1-MR and 2-MR PESs calculated by TD-DMRG with different bond dimension M_S. The analytically exact results with harmonic PES calculated by TVCF are also listed. A $100\,cm^{-1}$ Gaussian broadening is applied.

Method		$k_{ic}(\times 10^{10}\,s^{-1})$ at $0\,K$			$k_{ic}(\times 10^{10}\,s^{-1})$ at $300\,K$		
		HA	1-MR	2-MR	HA	1-MR	2-MR
TVCF		0.79	-	-	1.00	-	-
TD-DMRG	$M_S = 10$	0.60	1.27	2.92	0.78	1.65	3.80
	$M_S = 20$	0.74	1.42	3.23	0.88	1.77	4.10
	$M_S = 40$	0.78	1.47	3.40	0.96	1.85	4.19
	$M_S = 60$	0.79	1.47	3.54	0.97	1.86	4.37
	$M_S = 80$	-	-	3.56	-	-	4.53
relative value to HA		100%	186%	451%	100%	192%	467%

Furthermore, we examine the magnitude of the anharmonic effect with different energy gaps. Fig. 6 plots the IC rates on HA, 1-MR, and 2-MR PESs at 0 K and 300 K with different adiabatic energy gaps ΔE_{ad}. It shows that the size of the energy gap is very important for the anharmonicity to take effect. With a gap smaller than 1.6 eV, there is basically no anharmonic effect. With the increase of the gap, the anharmonic effect becomes more and more noticeable. The IC rate on HA PES decreases much faster than that on anharmonic 1-/2-MR PES with the increase of gap. This behavior, which has also been reported in the study of model molecules,[28] can be reasoned in this way: the larger the gap, the higher the energy level of the final vibrational state, and therefore the greater the anharmonic effect. Comparing the 1-MR and 2-MR PESs, the IC rate on 2-MR PES is faster. However, with an energy gap larger than 2.5 eV, the trend of the rate on 1-MR and 2-MR PESs to decrease as the gap increases seems comparable. In addition, at each energy gap, the anharmonic effect does not differ much at different temperatures.

To analyze the specific effects due to anharmonicity, the FSR IC rates are calculated at 0 K.
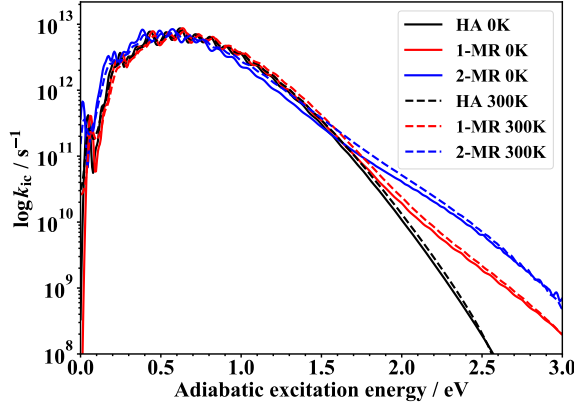
FIG. 6. k_{ic} of azulene on the HA (black), 1-MR (red), and 2-MR (blue) PESs at different S_0, S_1 adiabatic energy gaps. Solid line is $T = 0$ K, dashed line is $T = 300$ K.

The MPS to represent $|X_f(t)\rangle$ in Eq. (25) has $M_S = 20$, while MPSs to represent $\Gamma(t)$ and I_{half} have $M_S = 50$ (HA and 1-MR) and $M_S = 120$ (2-MR), respectively. In TD-DMRG, two primitive basis functions are used: one is SHO (used in HA PES), and the other is modal from VSCF calculation (used in 1-MR, 2-MR PESs). The primitive basis adopts $d = 10$ (the difference compared with $d = 20$ is very small). Since MPS is compressed in the calculation of $\Gamma(t)$ and I_{half}, to verify the accuracy, the total rate obtained by summing over the FSR rates $\sum_v I$ is listed in Table S1 and the total rate obtained directly by integrating $C(t)$ (in Table II) is the reference. From the comparison, the accuracy is sufficient for the later analysis of the FSR IC rates.

Based on the probability of different occupation numbers of each mode in Eq. (41) occurring in the total IC process, the mean vibrational quantum number and the mean accepting energy for each mode are defined as

$$\bar{v}_l = \sum_{v_l} p_{v_l} v_l \tag{42}$$

$$\bar{\varepsilon}_l = \sum_{v_l} p_{v_l} \varepsilon_{v_l} \tag{43}$$

where ε_{v_l} is $\omega_i v_i$ for the SHO basis function (not including the zero-point energy) and is the energy of each modal relative to the zero-point energy for the VSCF modal basis function. $\bar{v}_l$ on different PESs are shown in Fig. 7, in which the total $\bar{\varepsilon}_l$ of the 8 high-frequency C-H vibrations above 3000cm^{-1} ($\sum \bar{\varepsilon}_{C-H}$) are also listed. For HA PES, the modes with large HR factors receive more energy and the corresponding $\bar{v}_l$ is larger. The main contributor, mode 38, has the largest

21

2.4 mean vibrational quantum number, while the high-frequency C-H vibrations with small HR factors basically do not contribute, with a mean accepting energy of $1017\,\text{cm}^{-1}$, which in the later analysis is attributed to the energy received as a promoting mode. For 1-MR PES, $\bar{v}_l$ in the C-C vibrational region decreases significantly, with the largest being 1.9 (mode 38). This is mainly due to the significantly enhanced contribution of C-H vibrations, whose mean accepting energy is increased to $4680\,\text{cm}^{-1}$. From 1-MR PES to 2-MR PES, $\sum \bar{\varepsilon}_{\text{C-H}}$ increases further to $6309\,\text{cm}^{-1}$, and the corresponding $\bar{v}_l$ of C-C vibrations decreases further to a maximum of 1.5. Therefore, by introducing anharmonicity, the ability of C-H vibrations to receive electronic energy is opened up: on the original HA PES, C-H vibrations only receive less than $1/10$ of the electronic excitation energy, while they receive more than $1/3$ of the electronic excitation energy on the 2-MR PES. Since the C-H vibrations receive more energy, the quantum numbers of the C-C vibrations decrease. Qualitatively, according to that the FC factor between two displaced harmonic oscillators is $|\langle \chi_{i0} | \chi_{fv} \rangle|^2 = \frac{e^{-S} S^v}{v!}$ and for azulene HR factors are less than 1 (weak coupling regime), smaller v results in a larger FC factor and thus a faster IC rate after accounting for anharmonicity. However, for the 2-MR PES, the VSCF modals are used to approximate the final vibrational states. Hence, the statistical quantities in Eq. (42) (43) may be inaccurate. In order to check the reliability of this approximation on the statistical quantities, $\bar{v}_l$ of 1-MR, 2-MR PESs with SHO basis functions are shown in the Supporting Information Fig. S2. With SHO basis, $\bar{v}_l$ is also approximated on 1-MR PES. From Fig. S2, we find that $\bar{v}_l$ only changes a little on both 1-MR and 2-MR PESs with either SHO basis or modal basis. Therefore, the analysis of $\bar{v}_l$ and $\bar{\varepsilon}_l$ on 2-MR PES is reliable.

With the sampling algorithm described in the last section, the dominant final vibrational states that contribute the most to the total IC rate are analyzed. We find that unlike the statistical mean vibrational quantum number, the rate of individual final state is very sensitive to what kind of basis function is used. For 2-MR PES, the FSR rates obtained by using VSCF modal basis function are incorrect. Therefore, Fig. 8 only plots the results of HA PES with SHO basis and 1-MR PES with modal basis. A total of 10^5 final state configurations are sampled (the total number of configurations is 10^{48}). For HA(1-MR) PES, the contribution of the sampled configurations accounts for 91%(93%) of the total rate. This is an indication of the efficiency of our proposed sampling algorithm. In addition, it shows that the 10^5 configurations are sufficiently representative. The black bars in Fig. 8 are the rates of the top 1000 sampled configurations with the largest rates. Several configurations that contribute the most are labeled next to the bar. The blue curve is the rate-weighted density of states (DOS) calculated by the 10^5 configurations (a Gaussian broadening
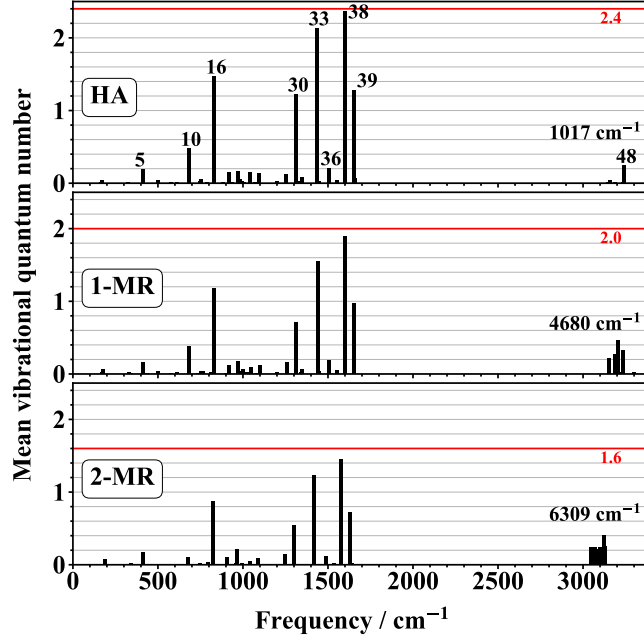
FIG. 7. The mean vibrational quantum number $\bar{v}_l$ received by each mode on the HA, 1-MR, and 2-MR ground state PESs, where HA uses SHO as the primitive basis function and 1-MR/2-MR use VSCF modal as the primitive basis function. The total mean accepting energy $\sum \bar{\varepsilon}_{\text{C-H}}$ of the C-H vibrations is also listed. The horizontal red line is a guide to the eye.

of $10\,\text{cm}^{-1}$ is used).

$$\rho(\omega) = \sum_i k_i \delta(\omega - \omega_i) \tag{44}$$

The overall FSR IC rates are increased in the 1-MR PES compared to HA PES. For HA PES, the configurations having a large rate are all composed of excited vibrations with large HR factors. Among them, the three configurations with the largest rates are $1_{16}1_{30}3_{33}4_{38}2_{39}$, $1_{16}1_{30}3_{33}5_{38}1_{39}$, $1_{16}2_{30}2_{33}4_{38}2_{39}$ (the subscript is the mode index). This result is consistent with the previous statistics of the mean vibrational quantum number. For the 1-MR PES, the three configurations with the largest rates become $1_{33}1_{38}4_{43}$, $1_{33}3_{38}3_{46}$, $2_{33}2_{38}3_{46}$ (the mode indices above 41 are all C-H vibrational modes), demonstrating that the rates of the final states with C-H vibrations excited increase greatly after considering the anharmonicity.

The increase of vibrational DOS on the anharmonic PES is also expected to be one factor that will increase the total IC rate, e.g., the DOS of Morse potential becomes larger with energy. To

23

further distinguish whether the increase in the total IC rate is due to the increase in the rate for each individual final state or the increase in the vibrational DOS, we calculate the DOS $\rho(\omega) = \sum_i \delta(\omega - \omega_i)$ for the sampled 10^5 states (using a $10\,\mathrm{cm}^{-1}$ Gaussian broadening). Actually, the DOS calculated here is an effective DOS, since only the sampled states with a not too small rate are counted. Fig. 9 shows that there is no fundamental difference between the DOS around the energy gap on HA PES and on 1-MR PES. The DOS is even slightly larger on HA PES. It confirms that the rate increases on anharmonicity PES is due to an increase in the rate of individual final state, such as the rate of C-H excited configurations, which originally have a small contribution on HA PES, increase considerably after considering anharmonicity.
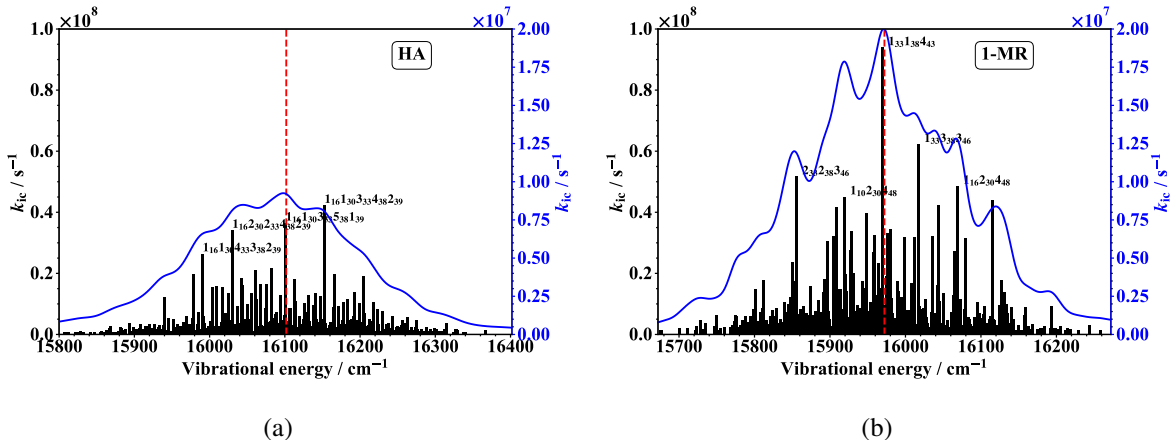

FIG. 8. The black bar is the rate of the top 1000 final configurations among the sampled 10^5 configurations and the blue curve is the rate-weighted density of states for the 10^5 final configurations (Eq. (44)) on (a) HA PES with SHO as the basis function and (b) 1-MR PES with modal as the basis function. The vertical red line indicates the 0-0 gap between the ground and excited states.

The following question is whether anharmonicity increases the ability of the C-H vibration to act as an accepting mode or a promoting mode. In the traditional understanding of the displaced harmonic oscillator model, since the C-H mode has an HR factor of about 0, it cannot be an accepting mode. Same results have been obtained for real molecular PESs with torsion and rotation.[59] To answer this question, we turn off the ability of the C-H vibration as a promoting mode, i.e., the NAC constants of all 8 C-H modes are set to 0. If the anharmonicity enhances the promoting ability of C-H vibration, the difference between the rates on anharmonic and harmonic PESs should be significantly reduced after turning off NAC of the C-H vibrations. From the total rates listed in Table III, although the total k_{ic} decreases after turning off NAC of C-H vibrations, the relative
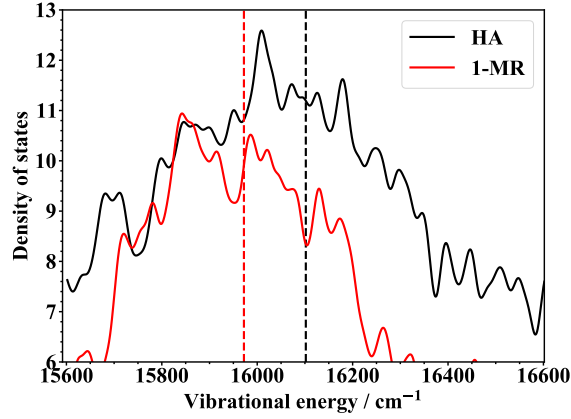
FIG. 9. Vibrational density of states $\rho(\omega) = \sum_i \delta(\omega - \omega_i)$ around energy gap for the sampled 10^5 configurations on the HA (black), 1-MR (red) PESs. The vertical line indicates the 0-0 gap between the ground and excited states.

value of k_{ic} on 1-MR and 2-MR PESs to that on HA PES is qualitatively unchanged. In addition, the mean accepting energy by C-H vibrations on 1-/2-MR PESs, which is the main factor on the change of IC rate, is also basically unchanged relative to that of HA PES. Similarly, Fig. 10 shows that without NAC of C-H vibrations, $\bar{v}_l$ of each mode on the 1-MR PES does not change much compared to that with C-H NAC. The situation is similar for the HA PES and 2-MR PES (see Fig. S3). These results demonstrate that the anharmonicity mainly enhances the accepting ability of C-H vibrations, even though the HR factor is ~ 0. Without anharmonicity, the C-H vibrations can only be the promoting mode, as $\sum \bar{\varepsilon}_{C\text{-}H}$ on HA PES decreases significantly from $1017\,\text{cm}^{-1}$ to $205\,\text{cm}^{-1}$ after turning off NAC of C-H vibrations.

TABLE III. The IC rate and mean accepting energy of C-H vibrations on HA, 1-MR and 2-MR PESs with and without nonadiabatic coupling of C-H vibrations at 0 K. ($M_S = 20$, $d = 10$)

PES	$k_{ic}(\times 10^{10}\,\text{s}^{-1})$		$\sum \bar{\varepsilon}_{C\text{-}H}\,(\text{cm}^{-1})$	
	with C-H NAC	without C-H NAC	with C-H NAC	without C-H NAC
HA	0.73	0.53	1017	205
1-MR	1.42 (195%)	1.09 (206%)	4680 (3663)	4065 (3860)
2-MR	3.25 (445%)	2.62 (494%)	6309 (5292)	6387 (6182)

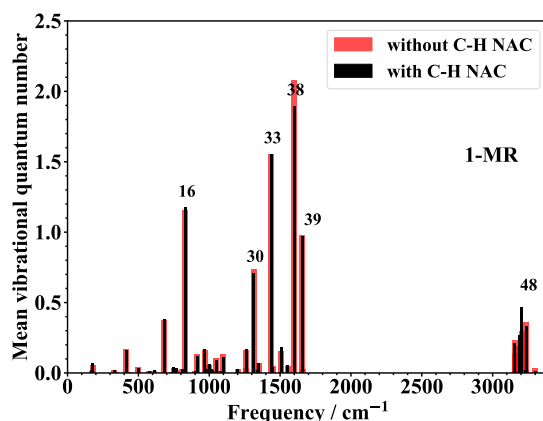We expect this specific anharmonic effect related to C-H vibrations to be general for the IC

25

FIG. 10. The mean vibrational quantum number of each mode with (black) or without (red) the nonadiabatic coupling of C-H vibrations on the 1-MR PES.

process of hydrocarbon compounds, at least for small-sized and medium-sized molecules. In experiments, it has already been observed that the number of C-H vibrations is very important to the nonradiative decay rate of hydrocarbons.[63] The most direct experimental verification of the effect of C-H vibrations on the nonradiative transition is the deuterium effect. When H is replaced by D, the frequency of the C-D vibration decreases, and thus the energy received by the same vibrational quantum number of C-D vibrations decreases. Therefore, the efficiency of C-H vibrations to accept energy is reduced and thus the rate of the nonradiative transition is expected to decrease. As early as the 1960s, experimental studies found that the lifetime of the triplet state of molecules such as naphthalene has a very pronounced deuterium effect. The lifetime of deuterated naphthalene becomes longer at low temperatures,[64] and many aromatic compounds other than naphthalene have similar phenomena.[65] Theoretically, the isotope effect of nonradiative transition rate has also been discussed qualitatively by Lin and Jortner *et al*.[17,66] According to the analytical rate expression of the displaced harmonic oscillator model under weak electron-vibrational coupling, the nonradiative transition rate is mainly determined by the highest-frequency mode with a nonzero HR factor, and the higher the frequency, the faster the rate. Therefore, under the assumption that the HR factor of C-H vibrations is not zero, it does exhibit a significant deuterium effect. What we find in this study is that for molecules like azulene, its C-H vibration can still get involved in nonradiative transition even though the HR factor is close to 0, and thus the molecule is expected to exhibit the deuterium effect as well. In addition, it was also found experimentally in naphthalene and acetophenone that the magnitude of deuterium effect only depends on the num-

26

ber of deuterium regardless of the substitution position.[66] According to the phenomena, Lin *et al.* qualitatively classified the C-H vibrations into the accepting modes, because if C-H vibrations are used as promoting modes, NAC may be sensitive to the positions of deuteration as the wavefunction varies over the molecule. On the contrary, due to the local nature of C-H vibrations, the C-H vibrational wavefunctions at different positions are similar and thus have similar abilities as accepting modes.[66] Our current quantitative calculations at ab initio level verify that the C-H modes are the accepting modes. However, it should also be noted that both experimental and theoretical studies showed that there is a low energy CI between S_1 and S_0 PESs in azulene, which is also important for the IC process.[55,67,68] The few nonadiabatic dynamics studies based on the trajectory surface hopping method have obtained an S_1 lifetime of 10 fs, which is much shorter than the experimental value.[67] Therefore, further theoretical studies are needed to properly understand the S_1 to S_0 IC process in azulene. Perhaps the contributions of both channels in the FC and CI regions need to be considered.[69]

IV. CONCLUSION AND OUTLOOK

To summarize, we present the methodology to calculate the internal conversion rate of real polyatomic molecules with an anharmonic potential energy surface at ab initio level in the Franck-Condon region by combining the n-MR method to construct PES and the TD-DMRG method to simulate quantum dynamics. Furthermore, a method to calculate the final-state-resolved rate coefficient is proposed, which is numerically exact for the uncoupled PES of the final state and helps in the analysis of the IC process. Taking the semi-rigid azulene molecule as an example, we compare and discuss in detail its IC rates on the harmonic potential, 1-MR potential, and 2-MR potential. We find that the anharmonic effect opens up the ability of the C-H vibration to receive electronic energy. Because the frequency of the C-H vibration is larger than that of the C-C vibration, the efficiency of receiving energy is higher. In the weak electron-vibrational coupling regime ($S_i < 1$), it is able to increase the Franck-Condon factor and thus increase the internal conversion rate. We expect this anharmonic effect to be prevalent in small-sized hydrocarbon compounds (small number of C-C vibrations). Whether this anharmonic effect is still present in large-sized hydrocarbon compounds (large number of C-C vibrations) deserves further investigation. Additionally, whether the 2-MR PES is accurate enough for rate calculations is unknown due to that 3-MR is too expensive to construct for such a system. There is still hope to combine with deep learning methods to

27

reduce the number of single-point calculations and obtain higher order of n-MR PES. Finally, the current method uses only rectilinear normal coordinates, which is not appropriate for very flexible molecules. Therefore, it is worth exploring a theoretical framework and computational method for nonradiative transition rate based on curvilinear coordinates.

ACKNOWLEDGMENTS

REFERENCES

[1] N. J. Turro, *Modern molecular photochemistry* (University science books, 1991).

[2] C. W. Tang and S. A. VanSlyke, "Organic electroluminescent diodes," Appl. Phys. Lett. **51**, 913–915 (1987).

[3] Z. Shuai and Q. Peng, "Organic light-emitting diodes: theoretical understanding of highly efficient materials and development of computational methodology," Natl. Sci. Rev. **4**, 224–239 (2017).

[4] T. R. Nelson, A. J. White, J. A. Bjorgaard, A. E. Sifain, Y. Zhang, B. Nebgen, S. Fernandez-Alberti, D. Mozyrsky, A. E. Roitberg, and S. Tretiak, "Non-adiabatic excited-state molecular dynamics: Theory and applications for modeling photophysics in extended molecular materials," Chem. Rev. **120**, 2215–2287 (2020).

[5] M. H. Beck, A. Jäckle, G. A. Worth, and H.-D. Meyer, "The multiconfiguration time-dependent hartree (mctdh) method: a highly efficient algorithm for propagating wavepackets," Phys. Rep. **324**, 1–105 (2000).

[6] S. M. Greene and V. S. Batista, "Tensor-train split-operator fourier transform (tt-soft) method: Multidimensional nonadiabatic quantum dynamics," J. Chem. Theory Comput. **13**, 4034–4042 (2017).

[7] Y. Yao, K.-W. Sun, Z. Luo, and H. Ma, "Full quantum dynamics simulation of a realistic molecular system using the adaptive time-dependent density matrix renormalization group method," J. Phys. Chem. Lett. **9**, 413–419 (2018).

[8] J. Zheng, J. Peng, Y. Xie, Y. Long, X. Ning, and Z. Lan, "Study of the exciton dynamics in perylene bisimide (pbi) aggregates with symmetrical quasiclassical dynamics based on the meyer–miller mapping hamiltonian," Phys. Chem. Chem. Phys. **22**, 18192–18204 (2020).

[9] X. Gao, Y. Lai, and E. Geva, "Simulating absorption spectra of multiexcitonic systems via quasiclassical mapping hamiltonian methods," J. Chem. Theory Comput. **16**, 6465–6480 (2020).

[10] X. Gao, Q. Peng, Y. Niu, D. Wang, and Z. Shuai, "Theoretical insight into the aggregation induced emission phenomena of diphenyldibenzofulvene: a nonadiabatic molecular dynamics study," Phys. Chem. Chem. Phys. **14**, 14207–14216 (2012).

[11] G. Cui and W. Thiel, "Generalized trajectory surface-hopping method for internal conversion and intersystem crossing," J. Chem. Phys. **141**, 124101 (2014).

[12] W. Zhou, A. Mandal, and P. Huo, "Quasi-diabatic scheme for nonadiabatic on-the-fly simulations," J. Phys. Chem. Lett. **10**, 7062–7070 (2019).

[13] D. Hu, Y. Xie, J. Peng, and Z. Lan, "On-the-fly symmetrical quasi-classical dynamics with meyermiller mapping hamiltonian for the treatment of nonadiabatic dynamics at conical intersections," J. Chem. Theory Comput. **17**, 3267–3279 (2021).

[14] R. Crespo-Otero and M. Barbatti, "Recent advances and perspectives on nonadiabatic mixed quantum–classical dynamics," Chem. Rev. **118**, 7026–7068 (2018).

[15] G. W. Robinson and R. Frosch, "Electronic excitation transfer and relaxation," J. Chem. Phys. **38**, 1187–1203 (1963).

[16] S. H. Lin, "Rate of interconversion of electronic and vibrational energy," J. Chem. Phys. **44**, 3759–3767 (1966).

[17] R. Englman and J. Jortner, "The energy gap law for radiationless transitions in large molecules," Mol. Phys. **18**, 145–164 (1970).

[18] M. Hayashi, A. Mebel, K. Liang, and S. Lin, "Ab initio calculations of radiationless transitions between excited and ground singlet electronic states of ethylene," J. Chem. Phys. **108**, 2044–2055 (1998).

[19] A. Mebel, M. Hayashi, K. Liang, and S. Lin, "Ab initio calculations of vibronic spectra and dynamics for small polyatomic molecules: Role of duschinsky effect," J. Phys. Chem. A **103**, 10674–10690 (1999).

[20]Q. Peng, Y. Yi, Z. Shuai, and J. Shao, "Excited state radiationless decay process with duschinsky rotation effect: Formalism and implementation," J. Chem. Phys. **126**, 114302 (2007).

[21]Q. Peng, Y. Yi, Z. Shuai, and J. Shao, "Toward quantitative prediction of molecular fluorescence quantum efficiency: role of duschinsky rotation," J. Am. Chem. Soc. **129**, 9333–9 (2007).

[22]Y. Niu, Q. Peng, and Z. Shuai, "Promoting-mode free formalism for excited state radiationless decay process with duschinsky rotation effect," Science in China Series B: Chemistry **51**, 1153–1158 (2008).

[23]Y. Niu, Q. Peng, C. Deng, X. Gao, and Z. Shuai, "Theory of excited state decays and optical spectra: application to polyatomic molecules," J. Phys. Chem. A **114**, 7817–7831 (2010).

[24]Z. Shuai, "Thermal vibration correlation function formalism for molecular excited state decay rates," Chin. J. Chem **38**, 1223–1232 (2020).

[25]C. Zhu, K. K. Liang, M. Hayashi, and S. H. Lin, "Theoretical treatment of anharmonic effect on molecular absorption, fluorescence spectra, and electron transfer," Chem. Phys. **358**, 137–146 (2009).

[26]R. Ianconescu and E. Pollak, "Semiclassical initial value representation study of internal conversion rates," J. Chem. Phys. **134**, 234305 (2011).

[27]R. Ianconescu, J. Tatchen, and E. Pollak, "On-the-fly semiclassical study of internal conversion rates of formaldehyde," J. Chem. Phys. **139**, 154311 (2013).

[28]A. Humeniuk, M. Buzancic, J. Hoche, J. Cerezo, R. Mitric, F. Santoro, and V. Bonacic-Koutecky, "Predicting fluorescence quantum yields for molecules in solution: A critical assessment of the harmonic approximation and the choice of the lineshape function," J. Chem. Phys. **152**, 054107 (2020).

[29]R. Valiev, R. Nasibullin, V. Cherepanov, G. V. Baryshnikov, D. Sundholm, H. Ågren, B. F. Minaev, and T. Kurtén, "First-principles calculations of anharmonic and deuteration effects on the photophysical properties of polyacenes and porphyrinoids," Phys. Chem. Chem. Phys. **22**, 22314–22323 (2020).

[30]Y. Wang, J. Ren, and Z. Shuai, "Evaluating the anharmonicity contributions to the molecular excited state internal conversion rates with finite temperature td-dmrg," J. Chem. Phys. **154**, 214109 (2021).

[31]V. Barone, "Anharmonic vibrational properties by a fully automated second-order perturbative approach," J. Chem. Phys. **122**, 014108 (2005).

[32] V. Barone, M. Biczysko, J. Bloino, M. Borkowska-Panek, I. Carnimeo, and P. Panek, "Toward anharmonic computations of vibrational spectra for large molecular systems," Int. J. Quantum Chem. **112**, 2185–2200 (2012).

[33] G. Li, C. Rosenthal, and H. Rabitz, "High dimensional model representations," J. Phys. Chem. A **105**, 7765–7777 (2001).

[34] J. M. Bowman, S. Carter, and X. Huang, "Multimode: a code to calculate rovibrational energies of polyatomic molecules," Int. Rev. Phys. Chem. **22**, 533–549 (2003).

[35] J. Behler, "Neural network potential-energy surfaces in chemistry: a tool for large-scale simulations," Phys. Chem. Chem. Phys. **13**, 17930–17955 (2011).

[36] L. Zhang, J. Han, H. Wang, R. Car, and E. Weinan, "Deep potential molecular dynamics: a scalable model with the accuracy of quantum mechanics," Phys. Rev. Lett. **120**, 143001 (2018).

[37] H. Wang and M. Thoss, "Multilayer formulation of the multiconfiguration time-dependent hartree theory," J. Chem. Phys. **119**, 1289–1299 (2003).

[38] C. Eckart, "Some studies concerning rotating axes and polyatomic molecules," Phys. Rev **47**, 552 (1935).

[39] J. R. Reimers, "A practical method for the use of curvilinear coordinates in calculations of normal-mode-projected displacements and duschinsky rotation matrices for large molecules," J. Chem. Phys. **115**, 9103–9109 (2001).

[40] A. Baiardi, J. Bloino, and V. Barone, "Accurate simulation of resonance-raman spectra of flexible molecules: An internal coordinates approach," J. Chem. Theory Comput. **11**, 3267–3280 (2015).

[41] A. Jäckle and H.-D. Meyer, "Product representation of potential energy surfaces," J. Chem. Phys. **104**, 7974–7984 (1996).

[42] U. Schollwöck, "The density-matrix renormalization group in the age of matrix product states," Ann. Phys. **326**, 96–192 (2011).

[43] J. Ren, W. Li, T. Jiang, and Z. Shuai, "A general automatic method for optimal construction of matrix product operators using bipartite graph theory," J. Chem. Phys. **153**, 084118 (2020).

[44] S. Paeckel, T. Köhler, A. Swoboda, S. R. Manmana, U. Schollwöck, and C. Hubig, "Time-evolution methods for matrix-product states," Ann. Phys. **411**, 167998 (2019).

[45] J. Haegeman, C. Lubich, I. Oseledets, B. Vandereycken, and F. Verstraete, "Unifying time evolution and optimization with matrix product states," Phys. Rev. B **94**, 165116 (2016).

[46] W. Li, J. Ren, and Z. Shuai, "Numerical assessment for accuracy and gpu acceleration of td-dmrg time evolution schemes," J. Chem. Phys. **152**, 024127 (2020).

[47] S. R. White, "Density-matrix algorithms for quantum renormalization groups," Phys. Rev. B **48**, 10345–10356 (1993).

[48] M. Zwolak and G. Vidal, "Mixed-state dynamics in one-dimensional quantum lattice systems: a time-dependent superoperator renormalization algorithm," Phys. Rev. Lett. **93**, 207205 (2004).

[49] A. E. Feiguin and S. R. White, "Finite-temperature density matrix renormalization using an enlarged hilbert space," Phys. Rev. B **72**, 220401 (2005).

[50] S. Carter, S. J. Culik, and J. M. Bowman, "Vibrational self-consistent field method for many-mode systems: A new approach and application to the vibrations of co adsorbed on cu (100)," J. Chem. Phys. **107**, 10458–10469 (1997).

[51] K. Boguslawski, K. H. Marti, and M. Reiher, "Construction of casci-type wave functions for very large active spaces," J. Chem. Phys. **134**, 224101 (2011).

[52] Z. Luo, Y. Ma, C. Liu, and H. Ma, "Efficient reconstruction of cas-ci-type wave functions for a dmrg state using quantum information theory and a genetic algorithm," J. Chem. Theory Comput. **13**, 4699–4710 (2017).

[53] M. Beer and H. Longuet-Higgins, "Anomalous light emission of azulene," J. Chem. Phys. **23**, 1390–1391 (1955).

[54] T. Itoh, "Fluorescence and phosphorescence from higher excited states of organic molecules," Chem. Rev. **112**, 4541–4568 (2012).

[55] E. W.-G. Diau, S. De Feyter, and A. H. Zewail, "Direct observation of the femtosecond non-radiative dynamics of azulene in a molecular beam: The anomalous behavior in the isolated molecule," J. Chem. Phys. **110**, 9785–9788 (1999).

[56] R. P. Steer, "Photophysics of molecules containing multiples of the azulene carbon framework," J. Photochem. Photobiol. C: Photochem. Rev. **40**, 68–80 (2019).

[57] M. J. Frisch, G. W. Trucks, H. B. Schlegel, G. E. Scuseria, M. A. Robb, J. R. Cheeseman, G. Scalmani, V. Barone, G. A. Petersson, H. Nakatsuji, X. Li, M. Caricato, A. V. Marenich, J. Bloino, B. G. Janesko, R. Gomperts, B. Mennucci, H. P. Hratchian, J. V. Ortiz, A. F. Izmaylov, J. L. Sonnenberg, D. Williams-Young, F. Ding, F. Lipparini, F. Egidi, J. Goings, B. Peng, A. Petrone, T. Henderson, D. Ranasinghe, V. G. Zakrzewski, J. Gao, N. Rega, G. Zheng, W. Liang, M. Hada, M. Ehara, K. Toyota, R. Fukuda, J. Hasegawa, M. Ishida, T. Nakajima, Y. Honda, O. Kitao, H. Nakai, T. Vreven, K. Throssell, J. A. Montgomery, Jr., J. E. Peralta,

F. Ogliaro, M. J. Bearpark, J. J. Heyd, E. N. Brothers, K. N. Kudin, V. N. Staroverov, T. A. Keith, R. Kobayashi, J. Normand, K. Raghavachari, A. P. Rendell, J. C. Burant, S. S. Iyengar, J. Tomasi, M. Cossi, J. M. Millam, M. Klene, C. Adamo, R. Cammi, J. W. Ochterski, R. L. Martin, K. Morokuma, O. Farkas, J. B. Foresman, and D. J. Fox, "Gaussian16 Revision C.01," (2016), gaussian Inc. Wallingford CT.

[58] Y. Niu, W. Li, Q. Peng, H. Geng, Y. Yi, L. Wang, G. Nan, D. Wang, and Z. Shuai, "Molecular materials property prediction package (momap) 1.0: a software package for predicting the luminescent properties and mobility of organic functional materials," Mol. Phys. **116**, 1078–1090 (2018).

[59] Y. Jiang, Q. Peng, X. Gao, Z. Shuai, Y. Niu, and S. H. Lin, "Theoretical design of polythienylenevinylene derivatives for improvements of light-emitting and photovoltaic performances," J. Mater. Chem. **22**, 4491–4501 (2012).

[60] O. Christiansen, "Midascpp," `https://gitlab.com/midascpp/midascpp`.

[61] M. Sparta, D. Toffoli, and O. Christiansen, "An adaptive density-guided approach for the generation of potential energy surfaces of polyatomic molecules," Theor. Chim. Acta **123**, 413–429 (2009).

[62] "Renormalizer," `https://github.com/shuaigroup/Renormalizer`.

[63] W. Siebrand, "Mechanism of radiationless triplet decay in aromatic hydrocarbons and the magnitude of the franckcondon factors," J. Chem. Phys. **44**, 4055–4057 (1966).

[64] C. A. Hutchison Jr and B. W. Mangum, "Effect of deuterium substitution on the lifetime of the phosphorescent triplet state of naphthalene," J. Chem. Phys. **32**, 1261–1262 (1960).

[65] R. Kellogg and R. Schwenker, ""temperature effect"on triplet state lifetimes in solid solutions," J. Chem. Phys. **41**, 2860–2863 (1964).

[66] S. H. Lin and R. Bersohn, "Effect of partial deuteration and temperature on tripletstate lifetimes," J. Chem. Phys. **48**, 2732–2736 (1968).

[67] M. J. Bearpark, F. Bernardi, S. Clifford, M. Olivucci, M. A. Robb, B. R. Smith, and T. Vreven, "The azulene s1 state decays via a conical intersection: a casscf study with mmvb dynamics," J. Am. Chem. Soc. **118**, 169–175 (1996).

[68] A. Wurzer, T. Wilhelm, J. Piel, and E. Riedle, "Comprehensive measurement of the s1 azulene relaxation dynamics and observation of vibrational wavepacket motion," Chem. Phys. Lett. **299**, 296–302 (1999).

[69]Q. Ou, Q. Peng, and Z. Shuai, "Toward quantitative prediction of fluorescence quantum efficiency by combining direct vibrational conversion and surface crossing: Bodipys as an example," J. Phys. Chem. Lett. **11**, 7790–7797 (2020).